JOURNAL OF SOLID STATE CHEMISTRY 87, 208–217 (1990)

Defect Structures in the Brannerite-Type Vanadates. IX. Preparation and Study of $Co_{1-y}Li_yV_{2-y}Mo_yO_6$ and $Co_{1-x-y}\phi_xLi_yV_{2-2x-y}Mo_{2x+y}O_6$ Solid–Solutions

BOGNA MASŁOWSKA AND JACEK ZIÓŁKOWSKI[1]

Institute of Catalysis and Surface Chemistry, Polish Academy of Sciences, 30-239 Kraków, ul. Niezapominajek, Poland

Received November 27, 1989

CoV_2O_6 doped with MoO_3 and Li_2O forms solid–solutions $CoLi\phi = Co_{1-x-y}\phi_xLi_yV_{2-2x-y}Mo_{2x+y}O_6$ (ϕ, cation vacancy in the original Co-position) belonging to the pseudoternary CoV_2O_6–$LiVMoO_6$–MoO_3 system. Particular cases are $CoLi = Co_{1-y}Li_yV_{2-y}Mo_yO_6$ ($x = 0$) and $Co\phi = Co_{1-x}\phi_xV_{2-2x}Mo_{2x}O_6$ ($y = 0$). Pure CoV_2O_6 is known to crystallize in two modifications: a low-temperature γ form stable below 660°C and a high-temperature α form of the brannerite-type structure (incongruent mp 740°C). Mo and Li doping stabilize the α form in such a way that the limit of the γ and/or $\gamma + \alpha$ range for $Co\phi$ and CoLi is at most $x = 0.02$ and $y = 0.05$, respectively. α-CoLi is thus stable at $x = 0$ for $0.05 < y \leq 1$. The opposite boundary of α-$CoLi\phi$ passes through the points (x; y): (0.22; 0), (0.37; 0.20), (0.31; 0.40), (0.24; 0.60), (0.16; 0.84). The phase diagram of the pseudobinary CoV_2O_6–$LiVMoO_6$ system (determined with DTA and X-ray analysis) shows (i) lens-type solidus–liquidus gap at high values of y, (ii) two peritectic meltings at lower y (yielding $Co_2V_2O_7$ and $Co_3V_2O_8$), and (iii) little area of γ and/or $\gamma + \alpha$ close to CoV_2O_6 in the subsolidus portion of the diagram. Lattice parameters are listed for CoLi which reveal negative deviations from Vegard's law. The obtained results are compared with data collected for the previously studied *Me*Li and *Me*Liϕ (*Me* = Mn, Zn, Mg). The radius of a cation vacancy in the brannerite-type structure is found to be smaller by 0.04–0.06 Å as compared to that of the exhausted cation.

1. Introduction

A number of bivalent metal vanadates MeV_2O_6 (*Me* = Mg, Mn, Co, Cu, Zn, Cd) crystallize in the monoclinic brannerite-type structure (labeled further as α) or it is exhibited by at least one of the polymorphs (*1*). In this structure (*2*), visualized in Fig. 1, distorted VO_6 octahedra sharing edges and corners form the anionic sheets parallel to (001), with tight packing along [010] and less tight packing along [100]. Me^{2+} cations situated also in distorted octahedra link the anionic layers in the [001] direction. The same structure is adapted by $LVMoO_6$ (*L* = Li, Na, Ag) compounds (*3, 4*).

In the present series of investigations (*5–14*) we have focused our attention on the solid–solutions of MoO_3 and Li_2O in the MeV_2O_6 brannerite-type matrices. The general formula of the solutions labeled *Me*Liϕ is $Me_{1-x-y}\phi_xLi_yV_{2-2x-y}Mo_{2x+y}O_6$; Mo^{6+} ions are substituted randomly for V^{5+} and similarly Li^+ and cation vacancies ϕ for Me^{2+}. Due to the stoichiometric limitation $MeLi\phi = (1 - x - y)\,MeV_2O_6 + y\,LiVMoO_6 + 2x\,MoO_3$. The discussed solutions belong thus to the pseudoternary

[1] To whom correspondence should be addressed.

0022-4596/90 $3.00

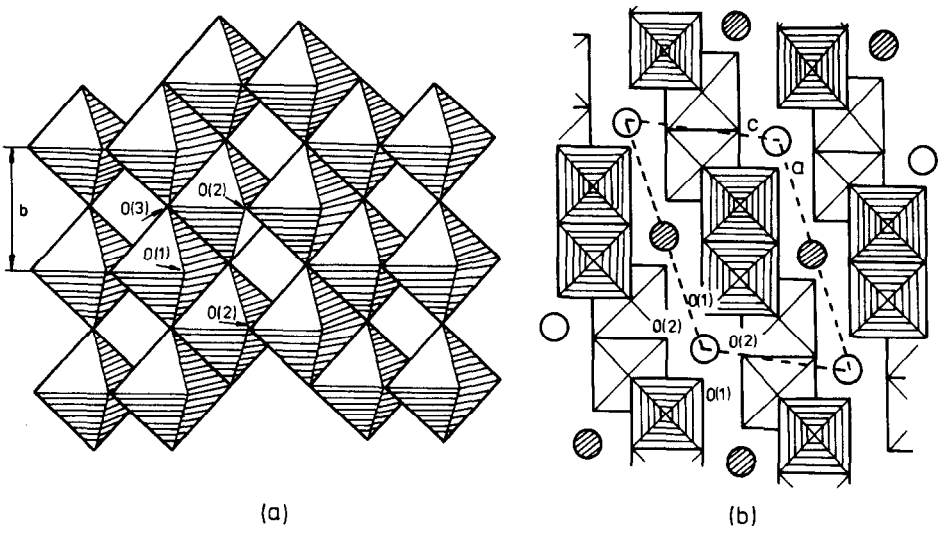

FIG. 1. Idealized outline of the brannerite-type MeV_2O_6 structure (after (*2*)). (a) A sheet of VO_6 octahedra parallel to (001) plane (nonequivalent oxygens linked with one, two, or three vanadium atoms are labeled 0(1), 0(2), and 0(3), respectively). (b) Projection of the structure on the (010) plane with marked *Me* cations and VO_6 groups on two different levels.

MeV_2O_6–$LiVMoO_6$–MoO_3 system. Their composition may be represented using the equilateral triangle with composition variables $X = 100x$ and $Y = 100y$ marked along MeV_2O_6–MoO_3 and MeV_2O_6–$LiVMoO_6$ arms, respectively (Fig. 2). *Me*Liϕ are known for *Me* = Mn, Zn, Mg (*9, 11, 12*) and the ranges of their stability are recalled in Fig. 2. With *Me* = Cu analogous $Cu^{2+}Cu^{+}\phi$ solid–solutions are formed (*7*) (cf. Fig. 2) in spite of the fact that $CuVMoO_6$ compound is unknown. Along the arms of the triangle pseudobinary solid–solutions exist which are extreme cases of *Me*Liϕ. These are

$Me\phi = Me_{1-x}\phi_xV_{2-2x}Mo_{2x}O_6$
(at $y = 0$, known for *Me* = Mn, Co, Zn (*5, 6, 10, 11*))

$MeLi = Me_{1-y}Li_yV_{2-y}Mo_yO_6$
(at $x = 0$, known for *Me* = Mn, Zn, Mg (*9, 11, 12*))

$Li\phi = Li_{1-x}\phi_xV_{1-x}Mo_{1+x}O_6$.
(at $x + y = 1$)

The latter solutions (Liϕ) have been earlier described in the literature (*3*) and confirmed in our work (*9, 11, 12*).

According to literature and our data (*10, 15–17*) CoV_2O_6 crystallizes in two modifications: a low-temperature γ form of unknown structure but of known X-ray pattern and a high-temperature α form of the brannerite-type structure with the transition temperature between 660 and 665°C. At 740°C peritectic melting of α-CoV_2O_6 yields $Co_2V_2O_7$ + liquid; at 830°C the next peritectic reaction gives $Co_3V_2O_8$ + liquid; the liquidus is crossed at 880°C.

It has been shown (*10*) that doping with MoO_3 as slight as $X = 2$ stabilizes the brannerite-type modification and α-Coϕ solid–solutions stable between room temperature and 520–740°C exist until $X = 22$. The relevant part of the T-CoV_2O_6-MoO_3 phase diagram is recalled in Fig. 5.

Verification of the possible existence of CoLi and CoLiϕ is the aim of the present work. We express the composition of the par-

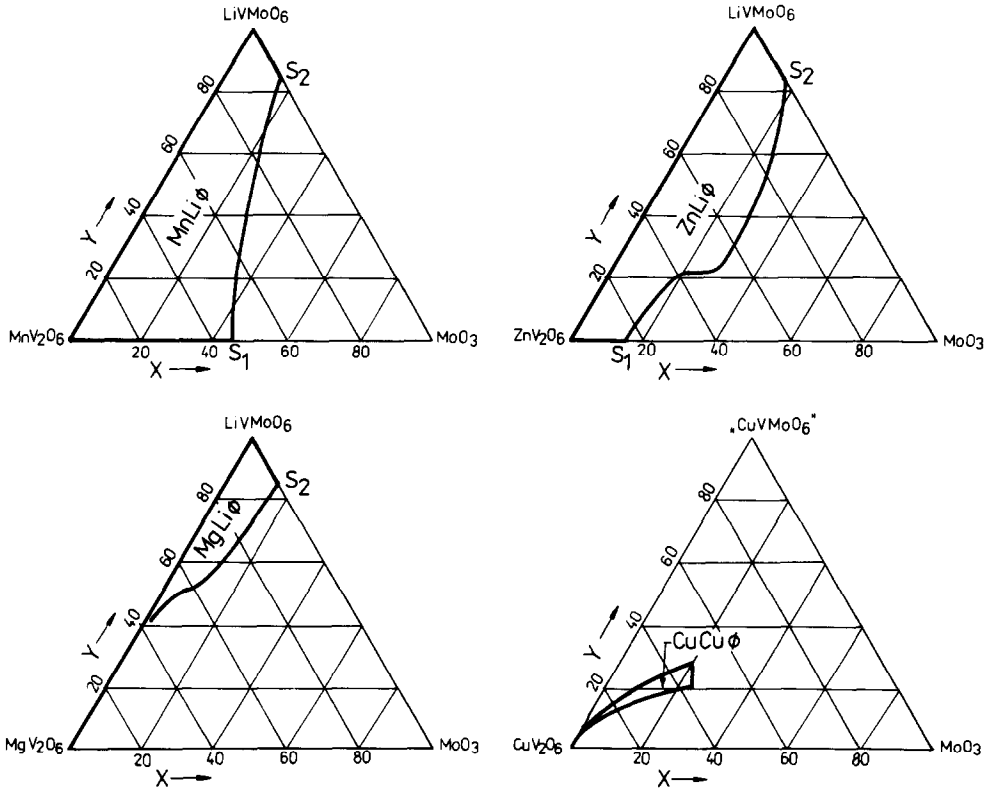

FIG. 2. Composition triangles and areas of stability of the previously studied solid-solutions: MnLiϕ (*9*), ZnLiϕ (*11*), MgLiϕ (*12*), CuCuϕ (*7*). The general formula of these solutions is $Me_{1-x-y}\phi_x Li_y V_{2-2x-y} Mo_{2x+y} O_6$ (Cu^+ appears instead of Li^+ in CuCuϕ). Coordinates used are $X = 100x$ and $Y = 100y$.

ticular sample by adding X and Y to the symbol; e.g., CoLiϕ-22-0 is equivalent to the saturated Coϕ solution of $x = 0.22$ and $y = 0$.

2. Experimental

Two methods were used to synthesize a number of samples of the CoLi and CoLiϕ composition. One of them involved solid state reactions between p.a. grade $(NH_4)_6 Mo_7O_{24} \cdot 4\ H_2O$, Li_2CO_3, "active" V_2O_5 (freshly precipitated from an aqueous solution of NH_4VO_3 with HNO_3, washed, dried at 120°C for 20 hr, and annealed at 500°C for 20 hr) and $CoCO_3 \cdot n\ H_2O$ (freshly precipitated from aqueous solutions of cobalt nitrate and sodium carbonate at 40–50°C, washed, and dried at 60°C for 20 hr). The content of oxides in the Co-, V-, and Mo-containing reactants was determined with gravimetric analysis (annealing until a constant weight); the content of Li in Li_2CO_3 was determined with potentiometric analysis. The weighted quantities of the reactants were ground and preheated in long quartz tubes at 580°C for 20 min to remove the volatiles. After grinding they were calcined at 620–640°C for 50 hr (the temperatures were so adjusted as to remain in a subsolidus range), quenched to room temperature, and examined with X-ray diffraction. Samples containing other phases beside brannerite were annealed again in the

same conditions to be sure that the equilibrium had been reached.

An alternative way of preparation of CoLi and CoLiϕ consisted in applying the amorphous citrate precursor methods (*18*) as adapted to our systems (*9*). The starting materials were p.a. grade NH_4VO_3, $(NH_4)_6Mo_7O_{24} \cdot 4H_2O$, $Co(NO_3)_2 \cdot 6H_2O$, Li_2CO_3 and citric acid. The cation content in the reactants was controlled as described above. Amorphous precursors were dried, preheated in a stream of air at 360–400°C for 12 hr (to combust the organic components), and finally annealed at 500°C for 70 hr.

The X-ray diffraction patterns were obtained with a DRON-2 diffractometer using Cu$K\alpha$ radiation, Ni filter, and an internal standard of Al (a = 4.0492 Å) at 25°C. The phase analysis was based upon the following literature data: γ-CoV_2O_6 (*15*), α-CoV_2O_6(*10*), $LiVMoO_6$ and Liϕ (*3, 4, 9*), a-$CoMoO_4$ (*19*), b-$CoMoO_4$ (*20*), V_2MoO_8 (*21*), V_2O_5 (*22*), MoO_3 (*23*). Lattice constants have been determined by least-squares method using 12–18 reflections (Latcon program, CERN library).

Elemental analysis (Pye-Unicam FP 90 spectrometer), DTA (Setaram M5 microanalyzer, 10°/min, Pt crucibles, samples of 12.5 mg), and the treatment of DTA curves were performed as described previously (*9, 10*).

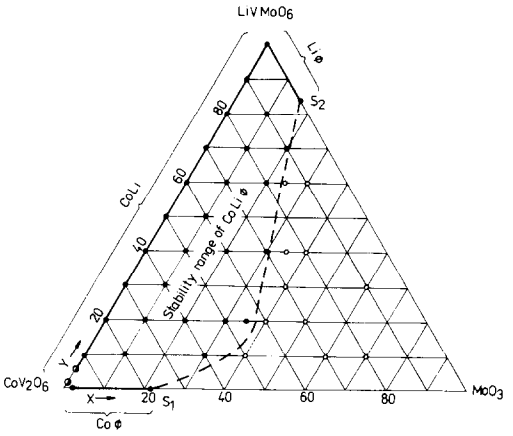

FIG. 3. The area of stability of the CoLiϕ solid–solution. Solid lines along the arms correspond to the stability ranges of Coϕ, CoLi, and Liϕ. Solid circles correspond to the studied samples composed of single brannerite-type phase. Open circles represent the studied samples more or less contaminated with other phases (MoO_3, V_2MoO_8, a-$CoMoO_4$, b-$CoMoO_4$, V_2O_5, and V_2O_5 doped with MoO_3). Close to the CoV_2O_6 corner a little area of γ and/or $\gamma + \alpha$ appears. A limit of this area has not been exactly determined due to the kinetic hindrance of the phase transformation (see text).

3. Results and Discussion

3.1. The Range of Stability of CoLiϕ

The composition of the studied CoLi and CoLiϕ samples is indicated in Fig. 3 (solid and open circles). It has been proven gravimetrically that during the thermal treatment there is no loss of material exceeding that expected due to the volatiles or combustion products. The elemental analyses of the chosen samples, performed after the final thermal treatment, also proved the intended stoichiometry. X-ray phase analysis revealed that all samples of the composition marked in Fig. 3 with solid circles give the pattern of pure brannerite, entirely indexable in a monoclinic system with systematic extinctions for $h + k = 2n + 1$. The range of stability of CoLiϕ is thus bordered by the "pentagon" extended between CoLiϕ-2-0 (limit of γ and/or $\gamma + \alpha$ range for (Coϕ), CoLiϕ-22-0 (S_1, saturated Coϕ), CoLiϕ-16-84 (S_2, saturated Liϕ), $LiVMoO_6$ and (about) CoLiϕ-0-5 (limit of γ and/or $\gamma + \alpha$ range for CoLi). The S_1S_2 line is strongly protuberant in the direction of the MoO_3 corner of the diagram. Samples of the composition marked in Fig. 3 with open circles and closer to the MoO_3 corner exhibited beside brannerite some other phases. Due to the overlapping of the X-ray reflections only MoO_3 and V_2MoO_8 have been identified without doubts. However, the presence of minor quantities of a-$CoMoO_4$, b-$CoMoO_4$, and V_2O_5 or rather a solid–solution of MoO_3

in V_2O_5 may not be excluded in some of samples. As we are essentially interested in the brannerite-type solid–solutions no detailed study of the diagram area close to the MoO_3 corner was undertaken.

The obtained results clearly demonstrate the large range of existence of CoLi and CoLiϕ and stabilization of the brannerite-type structure at the expense of the γ phase, not only on doping with Mo (*10*) but also with Mo + Li and Mo + Li + ϕ. However, the exact determination of the limit of γ form for CoLi and CoLiϕ is difficult. Freshly prepared samples CoLiϕ-0-2 and CoLiϕ-0-5 contained both modifications γ and α in the estimated quantities 90 + 10% and 20 + 80%, respectively. After few months of keeping at room temperature the content of α phase increased slightly at the expense of γ phase in both samples. This seems to indicate that the limit of stability of pure γ for CoLi is below $Y = 2$ and outside of it (perhaps until $Y = 5$) we deal with a range of coexistence of α and γ in which the equilibrium is reached with difficulty (due to kinetic hindrances or due to a minor nonhomogeneity).

3.2. *Lattice Constants of CoLi*

The determined lattice parameters of CoLi solid–solutions are listed in Table I and the parameter–composition plots for all *Me*Li solid–solutions studied so far are compared in Fig. 4. It is seen for CoLi that *b* and *a* increase linearly or almost linearly by 4.00 and 0.94%, respectively. This is due (i) to the substitution of the larger Mo^{6+} ion for the smaller V^{5+} (the ionic radii of Mo^{6+} and V^{5+} in octahedral coordination are 0.498 and 0.465 Å (*24*) or 0.59 and 0.54 Å (*25*), respectively; Co^{2+} and Li^+ ions are of more comparable size of 0.734 and 0.728 Å (*24*) or 0.745 and 0.76 Å (*25*), respectively), (ii) to the tightness of packing of the brannerite-type structure which is the highest along [010].

Parameters *c* and *c* sin β, reflecting the distance between the anionic layers, exhibit a pronounced minimum as a function of *y* thus indicating the negative deviation from Vegard's law. This accounts also for a slight but significant negative deviation of the dependence of the unit cell volume *V* on composition.

TABLE I

LATTICE PARAMETERS FOR THE CoLi = $Co_{1-y}Li_y$ $V_{2-y}Mo_yO_6$ SOLID–SOLUTIONS AND THEIR RELATIVE CHANGES $\Delta p\%$ BETWEEN THE END MEMBERS OF THE SERIES (STANDARD DEVIATION IS GIVEN IN PARENTHESES)

Y	*a* (Å)	*b* (Å)	*c* (Å)	β(°)	*c* sin β (Å)	*V* (Å^3)
0	9.251(2)	3.504(1)	6.618(2)	111.64(1)	6.152(2)	199.42
10	9.252(3)	3.523(2)	6.609(7)	111.83(2)	6.135(2)	199.97
20	9.260(2)	3.538(1)	6.606(1)	112.02(1)	6.124(1)	200.63
30	9.278(3)	3.562(1)	6.607(2)	112.12(1)	6.121(2)	202.29
40	9.284(3)	3.572(2)	6.601(1)	112.09(1)	6.116(1)	202.82
50	9.288(4)	3.588(3)	6.600(2)	112.09(1)	6.116(2)	203.82
60	9.300(1)	3.601(1)	6.608(1)	112.05(1)	6.125(1)	205.12
70	9.298(4)	3.605(3)	6.610(2)	112.02(2)	6.128(2)	205.40
80	9.324(1)	3.624(1)	6.620(1)	111.91(1)	6.142(1)	207.54
90	9.324(2)	3.634(1)	6.621(1)	111.79(1)	6.148(1)	208.32
100	9.338(5)	3.644(2)	6.632(4)	111.63(2)	6.165(4)	209.79
$\Delta p\%$	0.94	4.00	0.21		0.21	5.20

The results obtained for CoLi confirm the hypothesis formulated in Ref. (*11*), namely that the above-mentioned parameter–composition dependences (almost linear for *a* and *b* and negatively deviated for *c*, *c* sin β and *V*) are common for ZnLi, MgLi, and CoLi. This may be interpreted as a synergistic influence of the simultaneous presence of *Me* (Zn, Mg, or Co) and Li on the cohesion (stability) of the brannerite-type matrix. Due to this fact the *Me*Li matrix is able to tolerate an increased content of cation vacancies (CoLi $\rightarrow$ CoLiϕ, $X_{max} = 37$) as compared to the end members (CoV_2O_6 $\rightarrow$ Coϕ, $X_{max} = 22$; and $LiVMoO_6 \rightarrow$ Liϕ, $X_{max} = 16$) (let us remember that the composition parameter *X* is a measure of the content of vacancies in the lattice). As a result the boundaries S_1S_2 of the saturated *Me*Liϕ solid–solutions are strongly protuberant (cf.

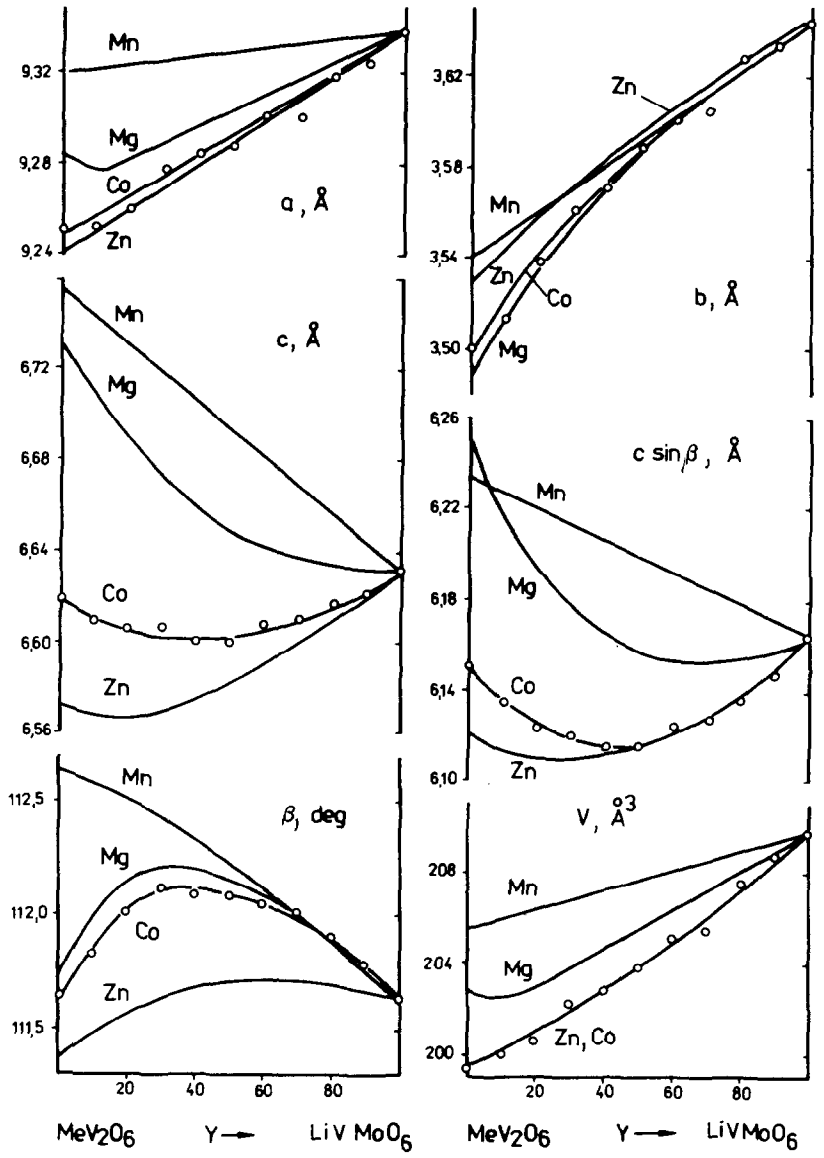

FIG. 4. Lattice parameters of CoLi solid–solutions as a function of composition (cf. Table I). For comparison the data for MnLi, ZnLi, and MgLi are included.

Figs. 2 and 3) in the direction of the MoO_3 corner of the diagram.

This is not the case with MnLi and MnLiϕ, where the lattice parameters of MnLi closely follow Vegard's law and the S_1S_2 phase boundary is slightly concave. The exceptional behavior of the Mn-containing phases may be related to the sizes of ions: the octahedral radii of Mg^{2+}, Co^{2+}, Zn^{2+}, and Li^+ are close (0.73–0.76) (*24*, *25*), while that of Mn^{2+} is about 10% larger. This may account for the energetically less con-

venient coexistence in the Li/Mn sublattice as compared to other Li/Me ones.

3.3. *The Size of Cation Vacancy*

In the previous paper (*11*) on the ZnLiϕ solid–solutions we have determined the lattice parameters of a number of samples (so called Q-series) the composition of which lay along a vertical line in the Zn V_2O_6–MoO_3–$LiVMoO_6$ diagram with (X, Y) from (0, 80) to (27.5, 25). Such samples have the constant concentration of vanadium ($2 - 2X - Y$) and molybdenum ($2X + Y$), but increasing concentration of vacancies (X) with the substitution of Zn^{2+} for Li^+, which are nearly of equal size. The changes of the lattice parameters along such a series and especially those of $c \sin \beta$ should be thus predominantly dependent on the "size" of the cation vacancy. The observed changes of $c \sin \beta$ along the above-mentioned Q-series have been then compared with the calculated values obtained by stacking of the regular octahedra built of ions of known radii (*24*). The comparison lead to the conclusion that the cation vacancy in ZnLiϕ behaves as an ion of the radius smaller by 0.06 Å as compared to the exhausted Li^+.

As the sizes of Co^{2+} and Li^+ are also comparable, the same can be done with CoLiϕ solutions. We have therefore determined the lattice parameters of CoLiϕ-30-20 (a = 9.317(3) Å, b = 3.609(2) Å, c = 6.618(2) Å, β = 112.11(2)°, $c \sin \beta$ = 6.131(2) Å) and compared them with those of CoLiϕ-0-80 (cf. Table I). With the analogous calculations as done for the Zn-containing Q-series we come to the conclusion that the radius of ϕ is smaller than that of Li^+ by 0.04 Å. This remains in good agreement with the former result for ϕ in ZnLiϕ.

3.4. *Phase Diagram of the CoV_2O_6–$LiVMoO_6$ System*

DTA of the CoLi samples revealed two endothermal effects. Effect I appearing between 651 and 740°C (depending on composition) was narrow, intense, and for some samples ($10 < Y < 50$) enriched with a shoulder (or poorly separated additional extremum). Diffused effect II followed the former at higher temperatures for $Y \leq 60$; its broadening increased with decreasing Y and two shoulders (or poorly separated additional extrema) were observed for $Y < 50$. The onset temperatures of the first effect and the endings of both of them have been determined accurately (±2°C). Positions of other subeffects were estimated tentatively. The phase diagram based on these data is shown in Fig. 5 (right). The identification of areas is based on the coincidence of the present diagram and that of the MoO_3–CoV_2O_6 system, studied previously (*10*) and recalled on the left of Fig. 5.

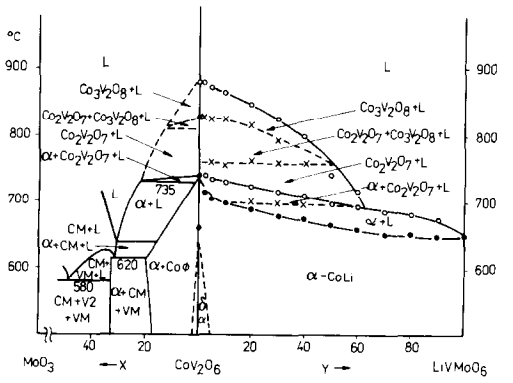

FIG. 5. Phase diagram of the pseudobinary Co V_2O_6–$LiVMoO_6$ system based on DTA (circles and crosses) and X-ray investigations ($\gamma + \alpha$ area). Solid circles, onset temperatures of endothermal effects; open circles, endings of endothermal effects; crosses, estimated positions of shoulders or poorly separated peaks. On the left the coincidence is shown with the previously determined (*10*) diagram of the MoO_3–CoV_2O_6 system. α-CoLi and α-Coϕ, brannerite-type solid–solutions (see text); CM, $CoMoO_4$; V2, V_2MoO_8; VM, V_2O_5-doped with MoO_3; L, liquid.

It is known from the X-ray studies that the narrow area of γ and/or $\gamma + \alpha$ phases exists close to CoV_2O_6; however, no DTA effects were observed in this range. Simi-

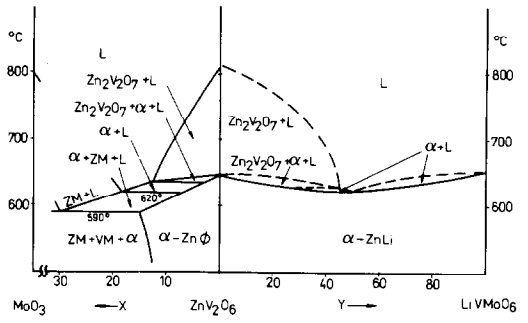

FIG. 6. Tentative phase diagram of the pseudobinary ZnV_2O_6–$LiVMoO_6$ system, constructed on the ground of (i) the former DTA (*11*), (ii) coincidence with MoO_3–ZnV_2O_6, given in the left part of the figure (*11*), (iii) analogy to the Co-containing system. α-ZnLi and α-Znφ, brannerite-type solid–solutions; ZM, $ZnMoO_4$; VM, V_2O_5 doped with MoO_3; L, liquid.

larly to the γ-Coφ/α-Coφ system (*10*) the γ-CoLi ⇆ α-CoLi transition is apparently too slow to be visualized with DTA.

The structure of the determined phase diagram is rather simple. With the exception of a little γ and/or γ + α range all the subsolidus belongs to the α-CoLi solid–solution which melts between 651 and 740°C depending on composition. On heating the samples of $10 < Y < 50$, before entire melting, we cross the areas of coexistence of (α + liquid), (α + $Co_2V_2O_7$ + liquid), ($Co_2V_2O_7$ + liquid), ($Co_2V_2O_7$ + $Co_3V_2O_8$ + liquid), and ($Co_3V_2O_8$ + liquid). For $50 < Y < 60$ two latter areas are omitted while for $0 < Y \leq 10$ the range (α + liquid) is omitted. For $Y > 60$ (α + liquid) transforms directly into pure liquid. It should be recalled after Refs. (*5* and *9*) that both the MoO_3–CoV_2O_6 and CoV_2O_6–$LiVMoO_6$ systems are only pseudobinary ones, therefore on heating the peritectic reactions take place yielding new phases which lie out of the basal composition scale. The considered systems belong in fact to the quaternary MeO–Li_2O–V_2O_5–MoO_3 system and some of the phase-boundary lines are a type of "projection" from the five-dimensional space.

3.5 Comparison of the MeV_2O_6–$LiVMoO_6$ (Me = Co, Zn, Mn) Phase Diagrams

In the previous work (*11*) we have demonstrated that ZnV_2O_6 and $LiVMoO_6$ display miscibility in the whole range of composition forming the ZnLi solid–solutions; only the melting points of these solutions have been determined, as recalled in Fig. 6 with a solid line. In view of the little differences between the melting points of ZnV_2O_6, $LiVMoO_6$, and ZnLi solid–solutions as well as the little width of the respective effects we were not able to construct in Ref. (*11*) a credible phase diagram of this system. Now, making use of (i) the comparison with diagrams of the MoO_3–CoV_2O_6 and CoV_2O_6–$LiVMoO_6$ systems, (ii) the principle of the coincidence of the MoO_3–MeV_2O_6 and Me V_2O_6–$LiVMoO_6$ diagrams, and (iii) former DTA curves, we have constructed a tentative phase diagram of the ZnV_2O_6-LiV MoO_6 system which is shown in Fig. 6.

For comparison the diagrams of the MoO_3–MnV_2O_6 and MnV_2O_6–$LiVMoO_6$ systems (including coincidence) are recalled in Fig. 7, after Refs. (*5* and *9*).

It results from Figs. 5–7 that the phase

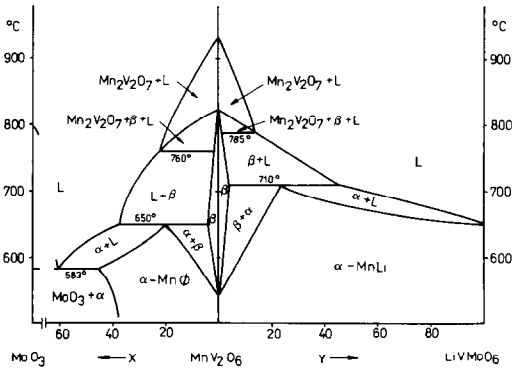

FIG. 7. Phase diagrams of the pseudobinary MoO_3–MnV_2O_6 and MnV_2O_6–$LiVMoO_6$ systems (after (*5*, *9*)).

diagrams of all three systems are highly analogous. Most of the subsolidus belongs to α-*Me*Li solid–solutions. At higher Y they melt through (α + liquid) to pure liquid thus revealing a lens type solidus–liquidus gap. At lower Y the α-*Me*Li solutions melt with peritectic decomposition, yielding $Me_2V_2O_7$, and (for *Me* = Co) $Me_3V_2O_8$ phases. The differences between the discussed diagrams are seen only close to MeV_2O_6 phases. They are due to the fact that α-CoV_2O_6 has a low-temperature polymorph, α-MnV_2O_6 has a high-temperature polymorph, and α-ZnV_2O_6 has no polymorphs (*1*).

4. Conclusions

CoV_2O_6 is known to crystallize in two modifications: a low-temperature γ-form stable until 660°C and a high-temperature α-form of the brannerite-type structure (incongruent mp 740°C). On doping CoV_2O_6 with MoO_3 and Li_2O solid–solutions CoLiϕ = $Co_{1-x-y}\phi_xLi_yV_{2-2x-y}Mo_{2x+y}O_6$ are formed belonging to the pseudoternary CoV_2O_6–Li $VMoO_6$–MoO_3 system. Particular cases are CoLi = $Co_{1-y}Li_yV_{2-y}Mo_yO_6$ (x = 0) and Coϕ = $Co_{1-x}\phi_xV_{2-2x}Mo_{2x}O_6$ (y = 0); the latter solution has been studied in Ref. (*10*). The indicated dopants stabilize the brannerite-type structure. The range of γ and/or γ + α does not exceed the limits $X = 100x = 2$ and $Y = 100y = 5$. Above $Y = 5$ (at $X = 0$) we deal with α-CoLi stable in the range $5 \leq Y \leq 100$. α-CoLi may be treated as a matrix able to incorporate an excess of Mo^{6+} ions compensated by the equivalent number of cation vacancies ϕ in the Co^{2+} sublattice, which results in formation of α-CoLiϕ. The stability range of α-CoLiϕ extends over about 50% of the area of the CoV_2O_6–$LiVMoO_6$–MoO_3 composition triangle and is bordered by a line passing through the points (X, Y); (22, 0); (37, 20); (31, 40); (24, 60); (16, 34). This boundary is strongly protuberant in the direction of the MoO_3 corner of the diagram which means that CoLi matrices tolerate much higher content of vacancies (X_{max} = 37) as compared to the end members CoV_2O_6 (X_{max} = 22) and $LiVMoO_6$ (X_{max} = 16). On the other hand lattice parameters show negative deviations from Vegard's law along the α-CoLi series of solid–solutions. Both the above-mentioned characters were also observed for *Me*Li and *Me*Liϕ containing Zn and Mg instead of Co. This may be interpreted as a synergistic influence of the simultaneous presence of *Me* (Co, Zn, Mg) and Li in the original *Me* sublattice on the cohesion of the brannerite-type matrix.

The phase diagram of the pseudobinary CoV_2O_6–$LiVMoO_6$ system has been determined and compared with those of Zn V_2O_6–$LiVMoO_6$ and MnV_2O_6–$LiVMoO_6$. The common features of all three diagrams are: lens-type solidus–liquidus gap at high values of Y and peritectic meltings at lower Y. Close to MeV_2O_6 the diagrams differ due to the fact that CoV_2O_6 and MnV_2O_6 have low-temperature and high-temperature modifications, respectively, while ZnV_2O_6 has no polymorphs.

The radius of the cation vacancy in the brannerite-type structure is found to be smaller by 0.04–0.06 Å as compared to that of the exhausted cation.

References

1. K. Mocała and J. Ziółkowski, *J. Solid State Chem.* **69,** 299 (1987) and papers quoted therein.
2. R. Ruh and A. D. Wadsley, *Acta Crystallogr.* **21,** 974 (1966).
3. J. Galy, J. Darriet, and B. Darriet, *C.R. Acad. Sci. Paris, Ser. C* **264,** 1477 (1967).
4. B. Darriet and J. Galy, *Bull. Soc. Fr. Mineral. Crystallogr.* **91,** 325 (1968).
5. R. Kozłowski, J. Ziółkowski, K. Mocała, and J. Haber, *J. Solid State Chem.* **35,** 1 (1980); erratum **38,** 138 (1981).
6. J. Ziółkowski, R. Kozłowski, K. Mocała, and J. Haber, *J. Solid State Chem.* **35,** 297 (1980).
7. T. Machej, R. Kozłowski, and J. Ziółkowski, *J. Solid State Chem.* **38,** 97 (1981).
8. R. Kozłowski and K. Stadnicka, *J. Solid State Chem.* **39,** 271 (1981).

9. J. ZIÓŁKOWSKI, K. KRUPA, AND K. MOCAŁA, *J. Solid State Chem.* **48,** 376 (1983).
10. K. MOCAŁA, J. ZIÓŁKOWSKI, AND L. DZIEMBAJ, *J. Solid State Chem.* **56,** 84 (1985).
11. K. MOCAŁA AND J. ZIÓŁKOWSKI, *J. Solid State Chem.* **71,** 426 (1987).
12. K. MOCAŁA AND J. ZIÓŁKOWSKI, *J. Solid State Chem.* **71,** 552 (1987).
13. K. MOCALA AND A. NAVROTSKY, *J. Solid State Chem.* **73,** 224 (1988).
14. K. MOCAŁA AND A. NAVROTSKY, *J. Solid State Chem.*, **80,** 45 (1989).
15. C. BRISI, *Ann. Chim.* **47,** 806 (1957).
16. E. E. SAUERBREI, M.S. thesis, McMaster Univ., Ontario, Canada (1972).
17. G. M. CLARK AND A. W. PICK, *J. Therm. Anal.* **7,** 289 (1975).
18. P. COURTY, H. AJOT, AND C. MARCILLY, *Powder Technol.* **7,** 21 (1973).
19. P. COURTINE, P. P. CORD, G. PANNETIER, J. C. DAUMAS, AND R. MONTARNAL, *Bull. Soc. Chim. Fr.* **12,** 4816 (1965).
20. G. W. SMITH AND J. A. IBERES, *Acta Crystallogr.* **19,** 269 (1965).
21. M. A. EICK AND L. KIHLBORG, *Acta Chim. Scand.* **20,** 1659 (1966).
22. H. G. BACHMAN, F. R. AHMED, AND W. H. BARNES, *Z. Kristallogr.* **115,** 110 (1961).
23. L. KIHLBORG, *Ark. Kemi.* **21,** 357 (1963).
24. J. ZIÓŁKOWSKI, *J. Solid State Chem.* **57,** 269 (1985).
25. R. D. SHANNON, *Acta Crystallogr. A* **32,** 751 (1976).